Cool La Niña During the Warmth of the Pliocene?
R. E. M. Rickaby, *et al.*
Science **307**, 1948 (2005);
DOI: 10.1126/science.1104666

(Fig. 4C). Comparison with the phase measured in the first pulse shows that the two measurements were correlated (Fig. 4D). In other words, the first measurement established a definite relative phase between the two condensates that may not have had a defined phase before, and the second measurement verified that the condensates evolved with that particular phase during the interval between pulses.

Interferometry was demonstrated by putting an interaction time between the two pulses and changing the outcome of the second measurement. We briefly modified the energy offset between the two wells during the interval between the pulses, when the phase was not being observed. Figure 4E compares the measured phase shift with the value $\Delta E \Delta t/h$ expected from an energy offset ΔE applied for a time Δt. The agreement between the prediction and the measurement demonstrates that the relative phase can be engineered by applying external forces to the atoms.

Active control of the phase opens interesting future perspectives: One could measure the light signal in real time and feed back the phase measurement into the control coils (or into the acousto-optical modulator that controls the two laser powers, creating the double-well potential), preparing the desired phase at the desired time. In principle, the uncertainty in the relative phase could even be squeezed by the feedback, allowing sub–shot noise interferometry (*5*, *10*, *30*).

Several physical interpretations of the experiment are possible besides the interference of two atom lasers. One is interference in momentum space (*21*): The zero-momentum component of the momentum distribution of the double condensate depends sinusoidally on the relative phase of the condensates and is probed with Doppler-sensitive spectroscopy (realized by Bragg scattering). Yet another point of view is that light scattering probes the excitation spectrum through the dynamical structure factor. The structure factor is phase-sensitive and shows interference fringes without requiring spatial overlap between the two condensates, as long as the excited states (after light scattering) have spatial overlap. This picture emphasizes that overlap between scattered atoms, as well as scattered photons, is crucial to our method: No phase information can be retrieved from two atomic wavepackets that scatter the same light but whose excited states are disconnected, like two condensates separated by a transparent glass wall.

The concept of beating atom lasers was previously exploited to measure spatial coherence in a single condensate (*31*) and for experiments done in optical lattices, where atoms outcoupled from a large vertical array of regularly spaced condensates interfered and their beating frequency measured gravity (*3*, *10*). In this case, condensates were split coherently by raising the optical lattice potential. Coupling was established by tunneling of atoms between adjacent lattice sites and depended exponentially on the barrier shape, whereas the laser beams in our scheme established a coupling through a state delocalized over the barrier. In principle, larger barriers could be overcome by imparting larger momenta in the Bragg process. From the standpoint of precision interferometry, optical lattices have the advantage of a very well-known and controlled displacement between condensates, whereas the optical detection that we introduce here measures the beat frequency continuously and in real time, with accuracy not depending on the calibration of image magnification (*3*) or other disturbances affecting atoms during time of flight.

Our scheme to nondestructively measure the beat frequency of two previously independent condensates, thus establishing phase coherence, could permit us to couple condensates displaced by tens of microns on atom chips or in other microtraps, to explore Josephson oscillations, phase diffusion, and self-trapping. We have already demonstrated its potential in exploiting the phase coherence of BECs to create a novel type of atom interferometer.

References and Notes

1. M. R. Andrews *et al.*, *Science* **275**, 637 (1997).
2. D. S. Hall, M. R. Matthews, C. E. Wieman, E. A. Cornell, *Phys. Rev. Lett.* **81**, 1543 (1998).
3. B. P. Anderson, M. A. Kasevich, *Science* **282**, 1686 (1998).
4. F. S. Cataliotti *et al.*, *Science* **293**, 843 (2001).
5. C. Orzel, A. K. Tuchman, M. L. Fenselau, M. Yasuda, M. A. Kasevich, *Science* **291**, 2386 (2001).
6. M. Greiner, O. Mandel, T. Esslinger, T. W. Hänsch, I. Bloch, *Nature* **415**, 39 (2002).
7. S. Gupta, K. Dieckmann, Z. Hadzibabic, D. E. Pritchard, *Phys. Rev. Lett.* **89**, 140401 (2002).
8. Y. Shin *et al.*, *Phys. Rev. Lett.* **92**, 050405 (2004).
9. Y. J. Wang *et al.*, preprint available at http://www.arxiv.org/abs/cond-mat/0407689 (2004).
10. M. A. Kasevich, *CR Acad. Sci. IV* **2**, 497 (2001).
11. C. CohenTannoudji, F. Bardou, A. Aspect, in *Laser Spectroscopy X*, M. Ducloy, E. Giacobino, Eds. (World Scientific, Singapore, 1992), p. 3.
12. K. Rzążewski, W. Żakovicz, *J. Phys. B* **25**, L319 (1992).
13. B. Dubetsky, P. R. Berman, *J. Mod. Opt.* **49**, 55 (2002).
14. J. Javanainen, *Phys. Rev. A* **54**, 4629(*R*) (1996).
15. A. Imamoglu, T. A. B. Kennedy, *Phys. Rev. A* **55**, 849(*R*) (1997).
16. J. Ruostekoski, D. F. Walls, *Phys. Rev. A* **56**, 2996 (1997).
17. J. Javanainen, S. M. Yoo, *Phys. Rev. Lett.* **76**, 161 (1996).
18. M. Naraschewski, H. Wallis, A. Schenzle, J. I. Cirac, P. Zoller, *Phys. Rev. A* **54**, 2185 (1996).
19. J. I. Cirac, C. W. Gardiner, M. Naraschewski, P. Zoller, *Phys. Rev. A* **54**, 3714(*R*) (1996).
20. Y. Castin, J. Dalibard, *Phys. Rev. A* **55**, 4330 (1997).
21. L. Pitaevskii, S. Stringari, *Phys. Rev. Lett.* **83**, 4237 (1999).
22. M. Kozuma *et al.*, *Phys. Rev. Lett.* **82**, 871 (1999).
23. J. Stenger *et al.*, *Phys. Rev. Lett.* **82**, 4569 (1999).
24. Information on materials and methods is available on *Science* Online.
25. A. Smerzi, S. Fantoni, S. Giovanazzi, S. R. Shenoy, *Phys. Rev. Lett.* **79**, 4950 (1997).
26. A. P. Chikkatur *et al.*, *Science* **296**, 2193 (2002).
27. M. Lewenstein, L. You, *Phys. Rev. Lett.* **77**, 3489 (1996).
28. J. Javanainen, M. Wilkens, *Phys. Rev. Lett.* **78**, 4675 (1997).
29. J. A. Wheeler, W. H. Zurek, *Quantum Theory and Measurement* (Princeton Univ. Press, Princeton, NJ, 1983).
30. J. M. Geremia, J. K. Stockton, H. Mabuchi, *Science* **304**, 270 (2004).
31. I. Bloch, T. W. Hansch, T. Esslinger, *Nature* **403**, 166 (2000).

32. This work was funded by the Army Research Office, the Defense Advanced Research Projects Agency, NSF, the Office of Naval Research, and NASA. M.S. acknowledges additional support from the Swiss National Science Foundation and C.S. from the Studienstiftung des deutschen Volkes. We thank G. Jo for experimental assistance, A. Schirotzek for contributions in the early stage of the work, and M. Zwierlein for a critical reading of the manuscript. We are indebted to A. Leanhardt for stimulating suggestions that initiated this research and insightful comments on the experiment and the manuscript.

Supporting Online Material

www.sciencemag.org/cgi/content/full/307/5717/1945/DC1

Materials and Methods

16 December 2004; accepted 3 February 2005

10.1126/science.1108801

Cool La Niña During the Warmth of the Pliocene?

R. E. M. Rickaby and P. Halloran

The role of El Niño–Southern Oscillation (ENSO) in greenhouse warming and climate change remains controversial. During the warmth of the early-mid Pliocene, we find evidence for enhanced thermocline tilt and cold upwelling in the equatorial Pacific, consistent with the prevalence of a La Niña–like state, rather than the proposed persistent warm El Niño–like conditions. Our Pliocene paleothermometer supports the idea of a dynamic "ocean thermostat" in which heating of the tropical Pacific leads to a cooling of the east equatorial Pacific and a La Niña–like state, analogous to observations of a transient increasing east-west sea surface temperature gradient in the 20th-century tropical Pacific.

In 1976, the equatorial Pacific, potentially driven by anthropogenic warming, switched from a weak La Niña state to one in which El Niño occurs with greater frequency and intensity (*1*). For the current climate system, El Niño years are warmer and La Niña years are cooler (*2*). In the future, more persistent El Niño could amplify global warming. Determining what drives ENSO and how

Department of Earth Sciences, University of Oxford, Parks Road, Oxford OX1 3PR, UK.

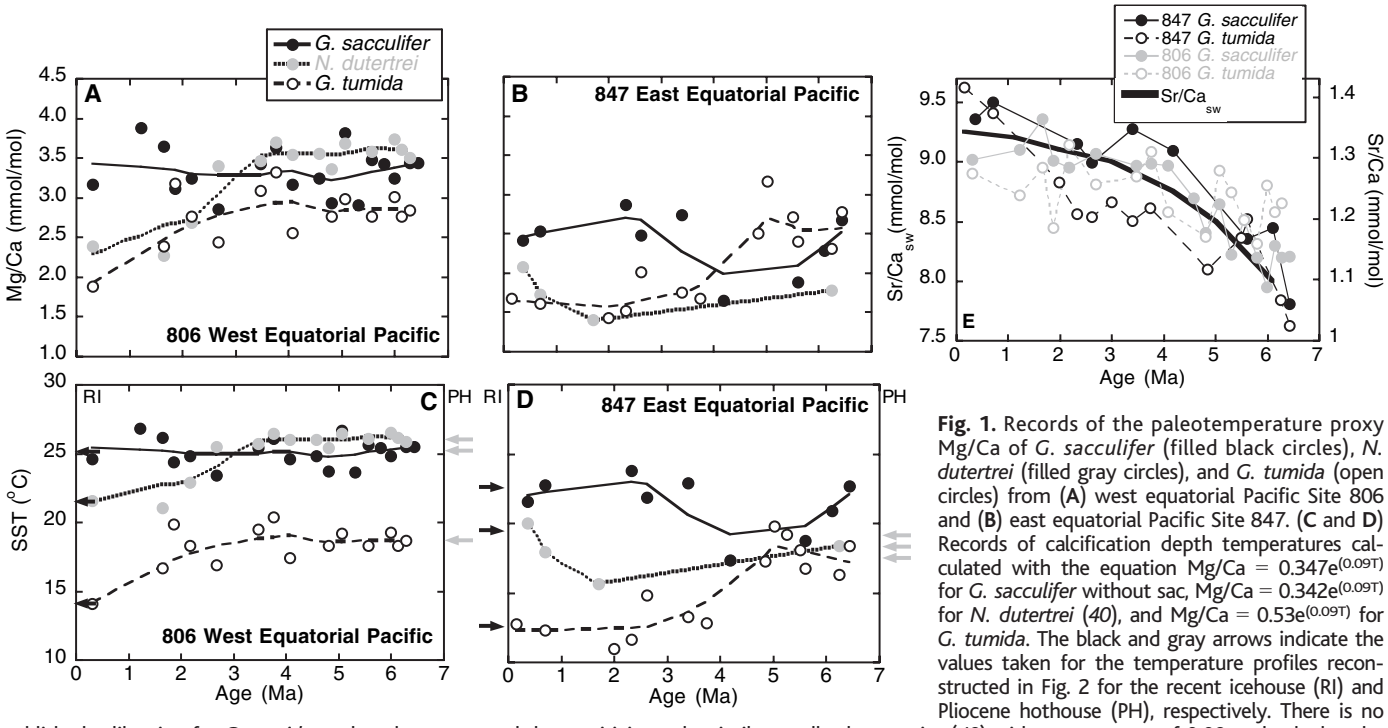

Fig. 1. Records of the paleotemperature proxy Mg/Ca of *G. sacculifer* (filled black circles), *N. dutertrei* (filled gray circles), and *G. tumida* (open circles) from (**A**) west equatorial Pacific Site 806 and (**B**) east equatorial Pacific Site 847. (**C** and **D**) Records of calcification depth temperatures calculated with the equation $Mg/Ca = 0.347e^{(0.09T)}$ for *G. sacculifer* without sac, $Mg/Ca = 0.342e^{(0.09T)}$ for *N. dutertrei* (*40*), and $Mg/Ca = 0.53e^{(0.09T)}$ for *G. tumida*. The black and gray arrows indicate the values taken for the temperature profiles reconstructed in Fig. 2 for the recent icehouse (RI) and Pliocene hothouse (PH), respectively. There is no published calibration for *G. tumida*, and we have assumed the sensitivity to be similar to all other species (*40*) with an exponent of 0.09 and calculated a pre-exponential constant of 0.53. This pre-exponential constant is similar to the calibrated pre-exponential constant for other deep dwellers such as *Globigerinella aequilateralis* and has been calculated with the consideration that most of the calcite is added as a keel at the base of the photic zone, i.e., ~ 200 m in the tropics (*38*). Our calibration for *G. tumida* is also constrained to provide a lower calcification temperature for *G. tumida* than for *G. sacculifer* (due to depth habit) at all times in all sites. The vital effects of deeper dwelling foraminifera can lead to increased incorporation of Mg at lower temperatures compared with shallower dwelling foraminifera (*40*). Our approach gives an accuracy of ±1.2°C in the estimation of calcification temperature but increases to ±3.0°C for *G. tumida*, given the uncertainty in the pre-exponential constant. The smoothed curve through each of the data sets represents a 50% weighted average. It seems reasonable to assume no change in seawater Mg/Ca during this period (*23*). (**E**) Records of Sr/Ca of *G. sacculifer* (filled circles), and *G. tumida* (open circles) from WEP Site 806 (gray) and EEP Site 847 (black) compared with whole-ocean change in Sr/Ca (*39*) to illustrate the minimal influence of dissolution.

the state of the Pacific thermocline has influenced past climates is critical to gain insight into Earth's response to future global warming.

The "hothouse" (*3*, *4*) climate of the early-mid Pliocene [~5 to ~2.7 million years ago (Ma), referred to as Pliocene] was the last extended period when global temperatures were warmer than present, peaking between 3 and 4 Ma, and provides an analog for a future global warming scenario. High-latitude air temperatures were ~10°C warmer (*4*), but tropical temperatures remained similar to today. Debate persists regarding the forcing of this warmth. Proxy-CO_2 reconstructions suggest that the perturbation was too small [~100 parts per million (ppm)] to effect such large changes in climate (*5*), and attention has focused on increased deep-ocean thermohaline circulation (*6*). Alternatively, teleconnections driven by the west equatorial Pacific warm pool (*7*) could propagate global warmth to induce a permanent El Niño–like state (*8*–*10*). The spatial climatic patterns of the "hothouse" largely resemble those of warm El Niño–like conditions (*10*), and there is $\delta^{18}O$ evidence for reduced thermocline tilt in the equatorial Pacific (*8*, *11*). However, the $\delta^{18}O$ of carbonate is controlled by the temperature and salinity of the water from which it precipitates. In the equatorial Pacific, zonal, depth, and seasonal variations in salinity have the potential to confound $\delta^{18}O$ temperature records. We use an independent record of surface and thermocline temperature, that is, Mg/Ca paleothermometry, to produce temperature records that, when used in conjunction with $\delta^{18}O$, yield a record of $\delta^{18}O_w$. We use these data to test the hypothesis that the Pacific collapsed onto a persistent El Niño–like state in the warm Pliocene.

Our records of Mg/Ca in three species of planktonic foraminifera from the east and west equatorial Pacific (EEP and WEP) (*12*) refute that El Niño–like conditions prevailed during the Pliocene hothouse (Fig. 1) (*8*, *11*). A feature of our temperature records is the divergence of surface and deeper water temperatures with time. *Globigerina sacculifer*, believed to calcify in the mixed layer, indicates that the sea surface temperature (SST) of the WEP warm pool remained relatively stable and consistently warmer than the EEP. The surface waters of the EEP warmed by ~5°C between 3 and 4 Ma. At each site, *Globorotalia tumida,* which adds calcite down to depths of 200 to 250 m, records a cooling of ~6°C. *Neogloboquadrina dutertrei*, with habitats ranging from 50 to 150 m, also shows a cooling trend similar to *G. tumida* in the WEP. The effects of dissolution are likely to be minimal (*13*).

We have reconstructed vertical profiles of contrasting cold Pleistocene and warm Pliocene surface hydrographies to show the evolution of the equatorial Pacific thermocline (Fig. 2). Between 3 and 4 Ma, the WEP thermocline shallowed. This cooling of subsurface waters could be related to the Cenozoic bottom-up cooling of the deep oceans and increased stratification in the Quaternary icehouse (*14*). By contrast, between 4 and 6 Ma in the EEP, the cold temperatures of the mixed layer and thermocline are identical, implying increased upwelling during the Pliocene. The EEP thermocline deepens to approach modern-day conditions.

Rather than indicating extreme El Niño–like conditions during hothouse climates evolving toward the modern east-west gradient in surface hydrography ~4 Ma (*8*, *10*), our data imply that the equatorial Pacific thermocline tilt was more extreme during the Pliocene, which indicates stronger trade winds, increased eastern upwelling, and La Niña–like conditions (*15*). Other evidence supports our notion. Aeolian sediments in the EEP sug-

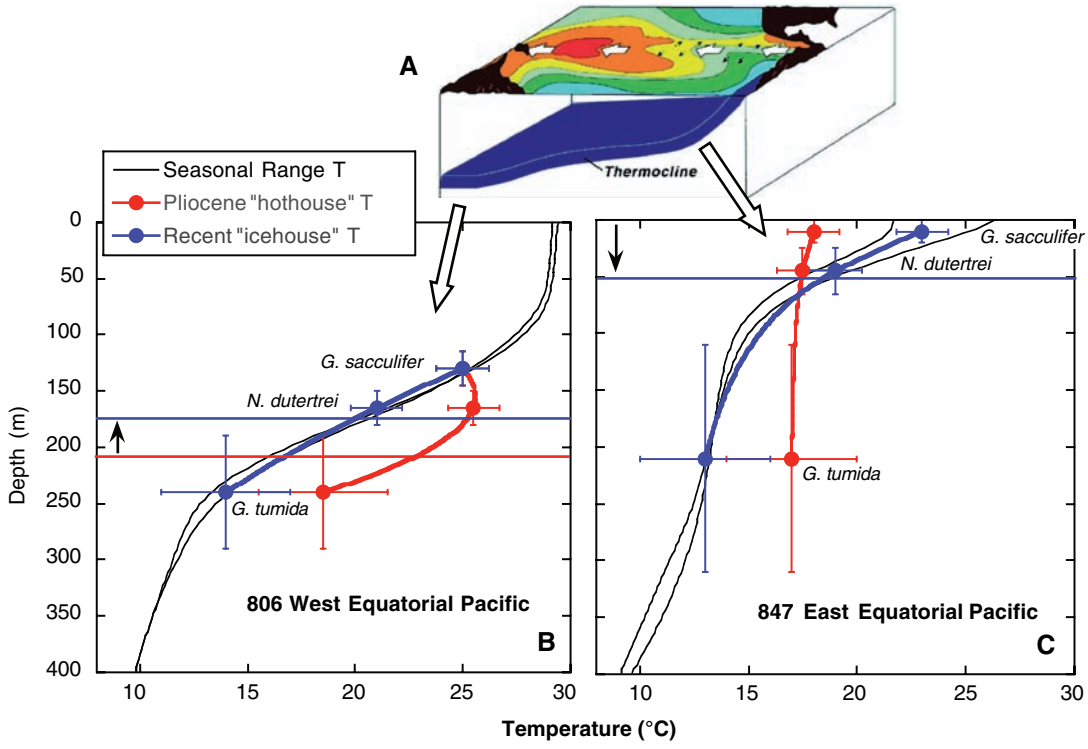

Fig. 2. (**A**) Schematic of the Pacific thermocline under normal conditions, illustrating the deepening beneath the west Pacific warm pool and shallowing to the east (adapted with permission from the Tropical Atmosphere Ocean Project, NOAA/Pacific Marine Environmental Laboratory). (**B** and **C**) Profiles of temperature derived from Mg/Ca for time-slice equivalents of the Pleistocene icehouse (0 to 1 My) in blue and the warm Pliocene (4 to 6 My) in red compared with the modern seasonal range in black taken from (*41*) for (B) WEP Site 806 and (C) EEP Site 847. The red and blue horizontal lines show the Pliocene and modern depths of the thermocline, and the black arrows indicate how this depth has changed since the Pliocene. We have used the modern seasonal temperature profile from (*41*) as a guide for habitat depth of each species. Error bars for *G. sacculifer* and *N. dutertrei* temperature reflect the quoted accuracy of ±1.2°C in the estimation of calcification temperature from published calibrations (*40*), which matches the scatter in our temperature records from the weighted average line from Fig. 1, C and D, and ±3.0°C for *G. tumida* to reflect the uncertainty in the pre-exponential constant. This envelope in temperature defines the depth error bar by comparison with the modern profiles, and we have assumed these errors to be the same for the Pliocene. The depth error bar encompasses the influence of a ~–2°C glacial cooling (*42*) on the modern temperature profile, which would result in an approximate 25 m shallowing of the thermocline (and our inferred depths) in both the EEP and the WEP. By comparison with (*41*), *G. sacculifer* consistently records colder temperatures than its mixed-layer habitat and appears to add calcite in the upper thermocline. *G. tumida* is described as a basal photic zone dweller. The tropical photic zone is deepest in the global ocean and is generally quoted at 200 m. *G. tumida* fits best with the modern-day temperature profile at a depth of 210 to 240 m, which is consistent with other observations that *G. tumida* can add calcite down to depths of 200 to 250 m (*43*). *N. dutertrei*, which is commonly described as a seasonal thermocline dweller associated with the deep chlorophyll maximum, calcifies at depths ranging from 60 to 150 m in the modern ocean. Compared with the modern profiles, the calcification temperature of *N. dutertrei* implies that it lives at 165 m in the WEP and at 45 m in the EEP. These depth habitats are also supported qualitatively by our reconstruction of $\delta^{18}O_w$ in Fig. 3.

gest very strong southeast trade winds 8 to 5 Ma, reducing in intensity until ~4 Ma (*16*). Higher rates of biogenic sedimentation occur along the equator during this interval (*17*) and reinforce our concept of increased divergent wind-driven upwelling enhancing productivity in the EEP prior to 4 Ma.

What could drive a La Niña–like state during Pliocene warmth? An "ocean thermostat" mechanism describes how greenhouse gas heating of the tropical Pacific leads to a cooling in the EEP (*18*, *19*), arising from the different SST response in the EEP and the WEP. In the west, where the thermocline is deep, the SST rises thermodynamically to attain a new equilibrium. In the east, where the thermocline is shallow, dynamic upwelling of cold waters counteracts the warming tendency. SST increases more in the west than in the east, enhancing the zonal temperature gradient. The atmosphere responds with increasing trade winds, which increase upwelling and thermocline tilt, cooling the surface waters in the east and further enhancing the temperature contrast. This "climatological" Bjerknes feedback reflects a shift in the mean state of the Pacific thermocline, which we invoke for our Pliocene La Niña–like state. External heating for a Pliocene feedback likely derives from a combination of greenhouse gases (~+100 ppm) and reduced planetary albedo due to enhanced oceanic heat transport to high latitudes (*5*, *6*). Alternative mechanisms to drive a persistent La Niña–like state or create a positive feedback to the Bjerknes mechanism are to enhance the thermocline tilt by increased flux of the Indonesian Throughflow (ITF) (*20*) or decrease the Pliocene temperature of the Equatorial Undercurrent (EUC), which ventilates the equatorial thermocline (*21*).

We reveal qualitative insight into the evolving character of the EUC by deconvolving the $\delta^{18}O_w$ ($\delta^{18}O_w$ of seawater) from existing $\delta^{18}O$ foraminifera data (*8*) using the Mg/Ca-derived temperature for each species (Fig. 3). The error in this $\delta^{18}O_w$ reconstruction from the combination of proxies is ~±0.6 (*22*), whereas whole-ocean $\delta^{18}O_w$ during this period is poorly constrained to be <0.5‰ (*23*), within the scatter of our data. At each Pacific site, the habitat of the deep dweller *G. tumida* stays at a relatively constant $\delta^{18}O_w$. In the WEP, *G. sacculifer* and *N. dutertrei* experience waters that are consistently isotopically heavier than *G. tumida*. This $\delta^{18}O_w$ signature implies that *G. sacculifer* captures the signature of the subsurface salinity maximum associated with the eastward thermocline flow of the EUC (Fig. 3C) by calcifying over a range in water depth, thus integrating the mixed layer and thermocline signatures (*24*, *25*). This is corroborated by the cooler-than-expected temperatures reconstructed from *G. sacculifer* Mg/Ca for the modern-day surface waters in the WEP (Fig. 2). There is a hint of an increase in $\delta^{18}O_w$ from *G. sacculifer* in the WEP over the past 2 million years (My), and from the *N. dutertrei* record in the EEP. The most striking feature, greater than the reconstruction error and modern seasonal variations, is the shift of $\delta^{18}O_w$ derived from *G. sacculifer* in the EEP from –0.6‰ in the Pliocene to 0.9‰ in the Pleistocene [equivalent to a Pliocene freshening of ~2.6 ± 1.8‰ (*26*)].

The surface waters of the EEP should experience a decrease in precipitation-evaporation (P-E) as the WEP "fresh pool" shifts westward in a La Niña–like Pliocene. Although Pliocene

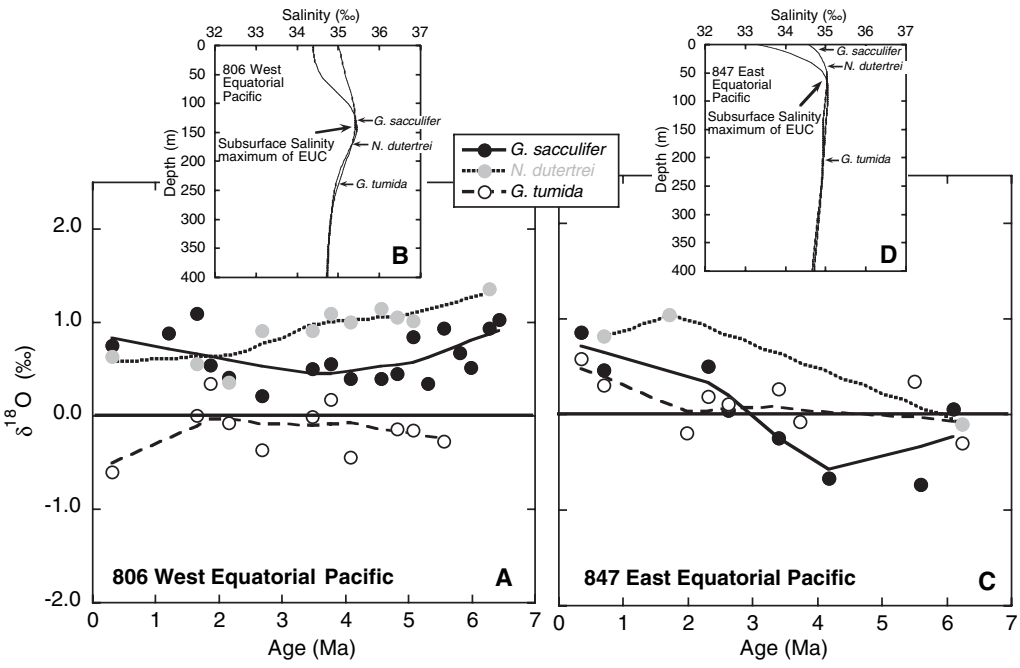

Fig. 3. The evolution of seawater $\delta^{18}O_w$ for *G. sacculifer* (black circles), *N. dutertrei* (gray circles), and *G. tumida* (open circles) from (**A**) Site 806 and (**C**) Site 847, calculated with the Mg/Ca calcification temperature and the paleotemperature equation T (°C) = 16.0 – 5.17 [$\delta^{18}O_c$ – ($\delta^{18}O_w$ – 0.27)] – 0.092[$\delta^{18}O_c$ – ($\delta^{18}O_w$ – 0.27)]^2, where the factor 0.27 was used to convert from water on the standard mean ocean water scale to calcite on the PeeDee Belemnite Scale. (**B** and **D**) Vertical profiles of the seasonal range in salinity (*41*) for (B) WEP Site 806 and (D) EEP Site 847. The likely depth habitats of the different species at each site are indicated. Although a quantitative reconstruction of paleosalinity from these combined proxy data is limited by likely error estimates between 0.6 and 1.8‰ (*26*), our reconstructed depth habits of *G. sacculifer* and *N. dutertrei* are strengthened by their reflection of more positive $\delta^{18}O_w$ values in the WEP, indicative of the subsurface salinity maximum.

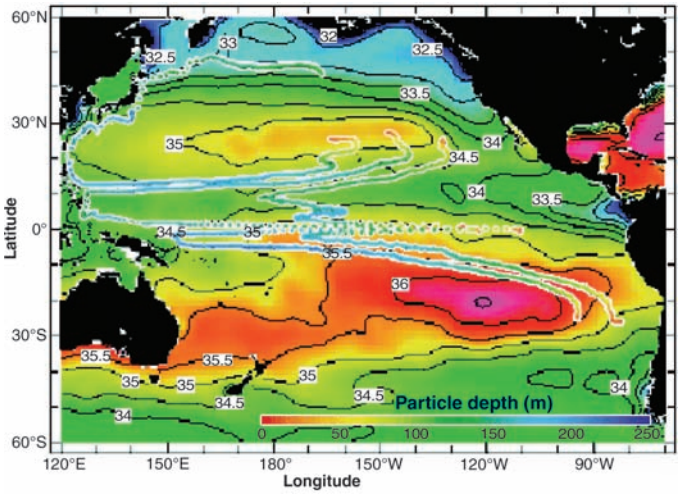

Fig. 4. A map of annual sea surface salinity (0-m depth) ranging from 32 to 37‰, showing contours every 0.5‰ or practical salinity unit (PSU) taken from (*41*) to illustrate the contrasting salinities in the northern and southern hemisphere source areas of water for the EUC. Also shown are selected paths of water parcels over a period of 16 years after subduction off the coasts of California and Peru, as simulated by means of a realistic general-circulation model forced with the observed climatological winds. From the colors, which indicate the depth of the parcels, it is evident that parcels move downward, westward, and equatorward unless they start too far west of California, in which case they join the Kuroshio Current. Along the equator, they rise to the surface while being carried eastward by the swift EUC, after (*21*).

precipitation is thought to have increased by ~5%, models suggest little change in P-E across the equatorial Pacific (*27*). The inference that *G. sacculifer* integrates a signature of the subsurface reconciles best our Mg/Ca-derived temperatures with existing studies of $\delta^{18}O$. *G. sacculifer* captures the nature of the EUC and records a change from cooler, fresher water during the Pliocene hothouse to warmer, saltier waters in the Quaternary icehouse. The increasing *G. sacculifer* $\delta^{18}O_w$ may be interpreted as a change in conditions of the source waters of the EUC from relatively cold and fresh during the Pliocene to warm and salty in the modern day. Today, the main subduction sites for surface waters entering the EUC are in the eastern and central South and North Pacific subtropical gyres and in the South and North Equatorial Currents (*20*, *28*); some typical pathways are shown in Fig. 4. Today, the contribution from warm and salty southern sources is more than double that of cool and fresh northern sources (*29*). To alter the character of the EUC to fresher and cooler during the Pliocene, either subtropical sources were fresher and cooler, or the dominant source of the EUC moved to higher latitudes, or the source changed from predominantly cold and fresh Northern hemisphere waters (NHW) during the Pliocene to warm and salty Southern hemisphere waters (SHW) today.

An interesting conjecture is that tectonic motions around the ITF switched the dominant source of the Pliocene EUC to be colder, fresher NHW (*9*, *29*). The emergence of Halmahera and the northward drift of New Guinea restricted the Indonesian seaway 3 to 4 Ma and diverted the ITF from 3°S to 2°N. The ITF plays an important role in determining the thermocline of the equatorial oceans. During the Pliocene, when the wider gateway caused a greater ITF flux, the contribution of cooler, fresher NHW dominated the Pacific EUC (*20*). Further, when the ITF opening is south of the equator, as in the Pliocene, warm and salty SHW tend to feed the ITF, and cold, fresh NHW supply the EUC. Conversely, when the opening is to the north, the ITF is primarily supplied by cold, fresh NHW, and there is a stronger southern component in the upwelling of the EEP.

We posit that the more southerly position of New Guinea ~5 Ma made cold, fresh NHW the dominant source of the EUC, which through upwelling in the EEP created an enhanced Bjerknes feedback, stronger southeasterly trade winds, Walker circulation, and a La Niña–like state. Can this La Niña–like state be reconciled with the warmer Pliocene climate?

The answer appears to be yes. Palaeoceanographic proxies suggest that deep thermohaline flow and heat transport to high latitudes was more vigorous during the Pliocene (*6*, *30*). Our proposed Pliocene La Niña–like state is consistent with elevated heat transport to high latitudes from two points of view. First, the reduced equator-pole temperature gradient of the Pliocene results in reduced intensity of Hadley cell circulation, a direct function of meridional pressure/temperature gradients (*31*).

Anomalies in the strength of the Hadley cells are inversely correlated with anomalies in the strength of the Walker oscillation (*18*, *31*): Weakened Hadley cells correlate with episodes of La Niña and strong Walker circulation. Second, the stronger oceanic heat flux to the high latitudes is consistent with enhanced Ekman flow of warm water poleward as a result of increased Walker circulation. The constraint of a balanced heat budget during the Pliocene implies that this increased heat loss at high latitudes through vigorous deep-ocean thermohaline circulation is accompanied by a shoaling of the tropical thermocline (*32*). Most oceanic heat gain occurs in low and mid-latitude upwelling zones and is large (small) when the thermocline is shallow (deep). During the Pliocene, the deeper thermocline in the WEP argues that thermocline tilt must be greater to allow shoaling of the EEP thermocline.

Our data rebut the hypothesis that "hothouse" climates collapse onto an El Niño–like state, in agreement with Eocene hothouse studies (*33*), and indicate that the tropical upper-ocean structure during the warm Pliocene was indicative of a La Niña–like state consistent with the dynamical "ocean thermostat." Twentieth-century global warming has also resulted in a stronger east-west SST gradient (*34*) on a contrastingly rapid time scale. Both of these scenarios, reflecting mean and transient Pacific states, respectively, support the role of the Bjerknes feedback inhibiting an El Niño positive feedback to global warming. Interestingly, during the Pliocene the increase in east-west SST gradient is due to eastern cooling, whereas during the 20th century it is due to WEP warming. In the near future, if the warming of the WEP warm pool reaches a limit without a compensating cooling in the east (afforded by the EUC during the Pliocene), could the Bjerknes feedback be reversed to incite accelerated warmth of an El Niño–like state?

References and Notes

1. W. J. Cai, P. H. Whetton, *Geophys. Res. Lett.* **27**, 2577 (2000).
2. K. E. Trenberth, D. P. Stepaniak, J. M. Caron, *J. Geophys. Res.* **107**, 4066 (2002); 10.1029/2000JD000297.
3. Here, we use "hothouse" to denote the warm early-mid Pliocene climate regime when the Northern Hemisphere lacked substantial ice sheets, and "icehouse" for the Middle to Late Pleistocene regime characterized by the waxing and waning of major Northern Hemisphere ice sheets.
4. M. Budyko, Y. A. Izrael, Eds., *Anthropogenic Climate Changes* (L. Gidrometeoizdat, Leningrad, 1987).
5. T. C. Crowley, *Quat. Sci. Rev.* **10**, 275 (1991).
6. M. E. Raymo, B. Grant, M. Horowitz, G. H. Rau, *Mar. Micropaleontol.* **27**, 313 (1996).
7. Global climate is influenced by the seesaw of the tropical Pacific thermocline tilt, or ENSO. This connection underpins the proposal of persistent El Niño conditions during geological "hothouse periods." The natural mode of oscillation is attributable to ocean-atmosphere interactions in which the trade winds create SST gradients that in turn reinforce the winds. In the Pacific, the prevailing easterly trade winds blow warm surface waters along the equator, creating a deep warm pool toward the western Pacific margin (*35*). This causes the tropical Pacific thermocline to become deeper in the west than in the east. Water is returned, along the thermocline, in the EUC, to the east, where it upwells. The zonal SST gradient between the west and east Pacific drives an east-west atmospheric circulation (the Walker Cell). This circulation further increases upwelling in the east Pacific, a process known as the Bjerknes feedback (*36*). Warm El Niño events occur when easterly trade winds decrease or reverse direction and warm water from the west Pacific spreads eastwards and, in doing so, reduces the Pacific thermocline tilt. This decreases the zonal temperature gradient, causing a breakdown of Walker Cell circulation. Cold La Niña events occur when trade winds are strong and induce a steep thermocline tilt. Changes in atmospheric circulation above the tropical Pacific cause changes in teleconnections to higher latitudes, with global climatic consequences on an interannual time scale. For this study, in which we investigate the average condition of the low-latitude ocean on million-year time scales, we refer to an El Niño (La Niña)–like state to reflect reduced (increased) east-west SST gradient, reduced (increased) thermocline tilt, and deeper (shallower) thermocline in the EEP. The detailed spatial patterns of atmosphere and ocean conditions associated with these two proposed states on geological time scales are currently unknown and may be very different from interannual configurations (*37*).
8. W. P. Chaisson, A. C. Ravelo, *Paleoceanography* **15**, 497 (2000).
9. M. A. Cane, P. Molnar, *Nature* **411**, 157 (2001).
10. P. Molnar, M. A. Cane, *Paleoceanography* **17**, 663 (2002); 10.1029/2001PA000663.
11. K. G. Cannariato, A. C. Ravelo, *Paleoceanography* **12**, 805 (1997).
12. Materials and methods are available as supporting material on *Science* Online.
13. At the critical site for our new interpretation, site 847, carbonate accumulation rates were higher prior to 4 Ma, which implies that preservation was improved during the Pliocene relative to today (*17*). The chemistry of *G. sacculifer* is insensitive to dissolution due to chemical homogeneity throughout the test (*38*). Planktonic Sr/Ca is a potential indicator of dissolution. Further evidence of the minimal influence of dissolution on these records is the covariation of Sr/Ca of *G. sacculifer* and *G. tumida* from both sites (Fig. 1E), which also parallels oceanic Sr/Ca evolution (*39*).
14. S. G. Philander, A. V. Federov, *Paleoceanography* **18**, 837 (2003); 10.1029/2002PA000837.
15. T. Izumo, J. Picaut, B. Blanke, *Geophys. Res. Lett.* **29**, 15073 (2002); 10.1029/2002GL015073.
16. S. A. Hovan, *Proc. ODP Sci. Results* **138**, 615 (1995).
17. T. King, *Mar. Micropaleontol.* **27**, 63 (1996).
18. A. C. Clement, R. Seager, M. A. Cane, S. E. Zebiak, *J. Clim.* **9**, 2190 (1996).
19. M. A. Cane *et al.*, *Science* **275**, 957 (1997).
20. K. B. Rodgers, M. A. Cane, N. H. Naik, D. P. Schrag, *J. Geophys. Res.* **104**, 20,551 (1999).
21. D. Gu, S. G. H. Philander, *Science* **275**, 805 (1997).
22. E. J. Rohling, *Mar. Geol.* **163**, 1 (2000).
23. C. H. Lear, Y. Rosenthal, J. D. Wright, *Earth Planet. Sci. Lett.* **210**, 425 (2003).
24. Y. Rosenthal, G. P. Lohmann, K. C. Lohmann, R. M. Sherrell, *Paleoceanography* **15**, 135 (2000).
25. H. J. Spero, K. M. Mielke, E. M. Kalve, D. W. Lea, D. K. Pak, *Paleoceanography* **18**, 1022 (2003); 10.1029/2002PA000814.
26. G. A. Schmidt, *Paleoceanography* **14**, 422 (1999).
27. L. C. Sloan, T. J. Crowley, D. Pollard, *Mar. Micropaleontol.* **27**, 51 (1996).
28. K. B. Rodgers *et al.*, *Geophys. Res. Lett.* **30**, 16003 (2003); 10.1029/2002GL016003.
29. K. B. Rodgers, M. Latif, S. Legutke, *Geophys. Res. Lett.* **27**, 2941 (2000).
30. K. Billups, A. C. Ravelo, J. C. Zachos, *Paleoceanography* **13**, 84 (1998).
31. A. H. Oort, J. J. Yienger, *J. Clim.* **9**, 2751 (1996).
32. G. Boccaletti, R. C. Pacanowski, S. G. H. Philander, A. V. Federov, *J. Phys. Oceangr.* **34**, 888 (2004).
33. M. Huber, R. Caballero, *Science* **299**, 877 (2003).
34. M. A. Cane, *Earth Planet. Sci. Lett.* **164**, 1 (2004).
35. E. Maier-Reimer, U. Mikalojewicz, T. J. Crowley, *Paleoceanography* **5**, 349 (1990).
36. A. V. Federov, G. Philander, *Science* **288**, 1997 (2000).
37. W. Hazeleger, R. Seager, M. A. Cane, N. H. Naik, *J. Phys. Oceanogr.* **34**, 320 (2004).
38. S. Brown, H. Elderfield, *Paleoceanography* **11**, 543 (1996).
39. C. H. Lear, H. Elderfield, P. A. Wilson, *Earth Planet. Sci. Lett.* **208**, 69 (2003).
40. P. Anand, H. Elderfield, M. H. Conte, *Paleoceanography* **18**, 846 (2003); 10.1029/2002PA000846.
41. S. Levitus, T. Boyer, *World Ocean Atlas 1994*, *Vol. 4*, NOAA National Environmental and Satellite Data and Information Service, U.S. Department of Commerce, Washington, DC (1994).
42. D. W. Lea, D. K. Pak, H. J. Spero, *Science* **289**, 1719 (2000).
43. E. C. Farmer, Thesis, Columbia University (2000).

44. We thank M. Evans and M. Cane for invaluable exchange of ideas, two anonymous reviewers who greatly improved this manuscript, J. Arden for technical support, and D. Sansom for art support. Further thanks to the Ocean Drilling Program for providing samples and to the Natural Environment Research Council for providing financial support.

Supporting Online Material

www.sciencemag.org/cgi/content/full/307/5717/1948/DC1
Materials and Methods
References

30 August 2004; accepted 24 January 2005
10.1126/science.1104666

Soft-Tissue Vessels and Cellular Preservation in *Tyrannosaurus rex*

Mary H. Schweitzer,[1,2,3]* Jennifer L. Wittmeyer,[1] John R. Horner,[3] Jan K. Toporski[4]†

Soft tissues are preserved within hindlimb elements of *Tyrannosaurus rex* (Museum of the Rockies specimen 1125). Removal of the mineral phase reveals transparent, flexible, hollow blood vessels containing small round microstructures that can be expressed from the vessels into solution. Some regions of the demineralized bone matrix are highly fibrous, and the matrix possesses elasticity and resilience. Three populations of microstructures have cell-like morphology. Thus, some dinosaurian soft tissues may retain some of their original flexibility, elasticity, and resilience.

A newly discovered specimen of *Tyrannosaurus rex* [Museum of the Rockies (MOR) specimen 1125] was found at the base of the Hell Creek Formation, 8 m above the Fox Hills Sandstone, as an association of disarticulated elements. The specimen was incorpo-